Rapid Kinetic Studies of Acetyl-CoA Synthesis: Evidence Supporting the Catalytic Intermediacy of a Paramagnetic NiFeC Species in the Autotrophic Wood−Ljungdahl Pathway†

Javier Seravalli, Manoj Kumar,‡ and Stephen W. Ragsdale*

Department of Biochemistry, Beadle Center, University of Nebraska, Lincoln, Nebraska 68588-0664

Received August 20, 2001; Revised Manuscript Received October 31, 2001

ABSTRACT: CO dehydrogenase/acetyl-CoA synthase (CODH/ACS), a key enzyme in the Wood−Ljungdahl pathway of anaerobic CO_2 fixation, is a bifunctional enzyme containing CODH, which catalyzes the reversible two-electron oxidation of CO to CO_2, and ACS, which catalyzes acetyl-CoA synthesis from CoA, CO, and a methylated corrinoid iron−sulfur protein (CFeSP). ACS contains an active site nickel iron−sulfur cluster that forms a paramagnetic adduct with CO, called the nickel iron carbon (NiFeC) species, which we have hypothesized to be a key intermediate in acetyl-CoA synthesis. This hypothesis has been controversial. Here we report the results of steady-state kinetic experiments; stopped-flow and rapid freeze-quench transient kinetic studies; and kinetic simulations that directly test this hypothesis. Our results show that formation of the NiFeC intermediate occurs at approximately the same rate as, and its decay occurs 6-fold faster than, the rate of acetyl-CoA synthesis. Kinetic simulations of the steady-state and transient kinetic results accommodate the NiFeC species in the mechanism and define the rate constants for the elementary steps in acetyl-CoA synthesis. The combined results strongly support the kinetic competence of the NiFeC species in the Wood−Ljungdahl pathway. The results also imply that the methylation of ACS occurs by attack of the Ni^{1+} site in the NiFeC intermediate on the methyl group of the methylated CFeSP. Our results indicate that CO inhibits acetyl-CoA synthesis by inhibiting this methyl transfer reaction. Under noninhibitory CO concentrations (below 100 μM), formation of the NiFeC species is rate-limiting, while at higher inhibitory CO concentrations, methyl transfer to ACS becomes rate-limiting.

The Wood−Ljungdahl (reductive acetyl-CoA) pathway plays an important role in the global carbon cycle. It is a mechanism for a number of anaerobic bacteria, including sulfate reducers, methanogens, and acetogens, to convert CO or CO_2 to cell carbon (*1*, *2*). Key enzymes involved in the acetyl-CoA pathway operate in reverse in some methanogens to convert acetic acid to methane (*3*). Unique aspects of the acetyl-CoA pathway include a preponderance of enzyme-bound one-carbon and two-carbon intermediates, the involvement of metal−carbon bonds at key steps, and a strategy of carbon−carbon bond formation that is similar to some well-studied organometallic reactions in solution (*4*).

The methyl group of acetyl-CoA is derived from CO_2. Through a series of transformations involving tetrahydrofolate (H_4folate)[1] enzymes, the one-carbon unit is reduced by six electrons to CH_3-H_4folate. Conversion of the methyl group of CH_3-H_4folate, CO_2, and CoA to acetyl-CoA is a remarkable series of reactions that are unique to anaerobic organisms that can use the Wood−Ljungdahl pathway (*1*). In the first reaction in this sequence, the methyl group of CH_3-H_4folate is transferred to a corrinoid iron−sulfur protein (CFeSP) by an enzyme called methyltransferase (MeTr) to form methyl corrinoid species (*5*), the first in a series of organometallic intermediates. The CFeSP (*6*) and MeTr (*7*, *8*) have been cloned, sequenced, and overexpressed in *Escherichia coli*, and the X-ray structure of MeTr is known (*9*). Besides the corrinoid cofactor, the CFeSP contains a low-potential $[Fe_4S_4]^{2+/1+}$ cluster, whose role is to mediate the transfer of electrons between external electron donors and the corrinoid cofactor (*10*, *11*).

Conversion of the methyl group of the methylated CFeSP to the methyl group of acetyl-CoA occurs through a series of intermediates that are bound to a bifunctional nickel iron−sulfur enzyme named carbon monoxide dehydrogenase/acetyl-CoA synthase (CODH/ACS) (*4*). A NiFeS cluster on CODH, which is called cluster C, catalyzes the reversible reduction of CO_2 to CO (eq 1), whereas a separate NiFeS cluster on ACS, called cluster A, catalyzes the condensation

† This work was supported by NIH Grant GM39451.

* To whom correspondence should be addressed. Phone: 402-472-2943. Fax: 402-472-8912. E-mail: sragsdale1@unl.edu.

‡ Present address: Genencor International, Inc., 925 Page Mill Road, Palo Alto, CA 94304.

[1] Abbreviations: H_4folate, tetrahydrofolate; HPLC, high-performance liquid chromatography; RCQ, rapid chemical quench; RFQ, rapid freeze quench; Tris, tris(hydroxymethyl)aminomethane; CODH/ACS, carbon monoxide dehydrogenase/acetyl-CoA synthase; CFeSP, corrinoid iron−sulfur protein; NiFeC, nickel−iron−carbon species; MeTr, methyltetrahydrofolate:corrinoid iron−sulfur protein methyltransferase; MES, 2-morpholinoethanesulfonic acid; PCA, protocatechuic acid (3,4-dihydroxybenzoic acid); PCD, protocatechuic acid dioxygenase; CoA, coenzyme A; DTT, dithiothreitol; C_{int} and C_{red2}, one-electron reduced and two-electron reduced forms of cluster C on CODH.

10.1021/bi011687i CCC: $22.00
Published on Web 01/16/2002

of CO, a methyl group, and CoA to form acetyl-CoA (eq 2). A third $[Fe_4S_4]^{2+/1+}$ exists on CODH, which is known as cluster B. This cofactor has the spectroscopic properties of a typical clostridial ferredoxin-type cubane cluster. Finally, recent X-ray crystallographic studies have revealed the presence of another $[Fe_4S_4]^{2+/1+}$ cluster, which has been named cluster D (*12*, *13*).

$$CO_2 + 2e^- + 2H^+ \overset{\text{CODH}}{\rightleftharpoons} CO + H_2O \qquad (1)$$

$$CH_3\text{-CFeSP} + CO + CoA \overset{\text{ACS}}{\rightleftharpoons} CH_3{-}CO{-}SCoA + H^+ + CFeSP \qquad (2)$$

When CO is reacted with CODH/ACS, a slow relaxing EPR signal is observed with *g*-values at 2.08, 2.07, and 2.03 that is called the NiFeC signal (*14*). Fourier transform infrared (FTIR) spectroscopic studies have demonstrated that CO is terminally bound to one of the metals in cluster A (*15*). EPR (*16*) and Mössbauer (*17*, *18*) studies have shown that the species eliciting the NiFeC signal contains a diamagnetic $[Fe_4S_4]^{2+}$ cluster that is exchange coupled to a paramagnetic Ni^{1+} site.

Under most growth conditions, CODH catalyzes the reduction of CO_2 to CO, which becomes the carbonyl group of acetyl-CoA (*19*). The CODH and ACS reactions are kinetically coupled by a channel that facilitates delivery of the product of the CODH reaction (CO) to cluster A where it reacts with the methylated CFeSP and CoA (*20*, *21*). This reaction sequence is summarized in Figure 1. Several aspects of this reaction are not known and some are controversial. Although the reaction sequence is written in the order (i) ACS−CO, (ii) CH_3-ACS−CO, (iii) acetyl-ACS, (iv) acetyl-CoA, it is not clear whether methyl transfer or CO binding to ACS occurs first. The oxidation state of cluster A, especially that of the Ni atom, during the catalytic cycle is actively discussed and is a major focus of this paper.

There are two competing hypotheses for acetyl-CoA synthesis. In the "paramagnetic catalytic cycle" (Figure 1a), the key intermediate 1 is the EPR-active NiFeC species (*16*, *22*). In the "diamagnetic catalytic cycle" (Figure 1b), all intermediates are diamagnetic and the NiFeC species is not part of the catalytic cycle (*23*).

Several results support the intermediacy of the NiFeC species. The "carbon" in the NiFeC species undergoes exchange with the carbonyl group of acetyl-CoA (*15*, *24*). When CO is reacted with CODH/ACS, the NiFeC EPR signal (*24*, *25*) forms fast enough to support the carbonyl exchange between acetyl-CoA and free CO, when measured under similar conditions. The NiFeC signal also is formed from acetyl-CoA through a reversal of the pathway (*24*) and from CO_2 under reducing conditions (*26*). The proportion of NiFeC species obtained at saturating CO concentrations (0.3−0.5 spin per mole of dimeric enzyme) equals the fraction of "labile" active nickel (measured by *o*-phenanthroline treatment) (*23*) and the equivalents of CoA (*27*) and methyl groups (*23*) that can bind to ACS.

However, several results appear to be inconsistent with the paramagnetic catalytic cycle. Although rates were not measured, when the paramagnetic NiFeC state of ACS is reacted with the methyl donor, the EPR signal disappears (*23*, *28*). Grahame concluded that this paramagnetic species

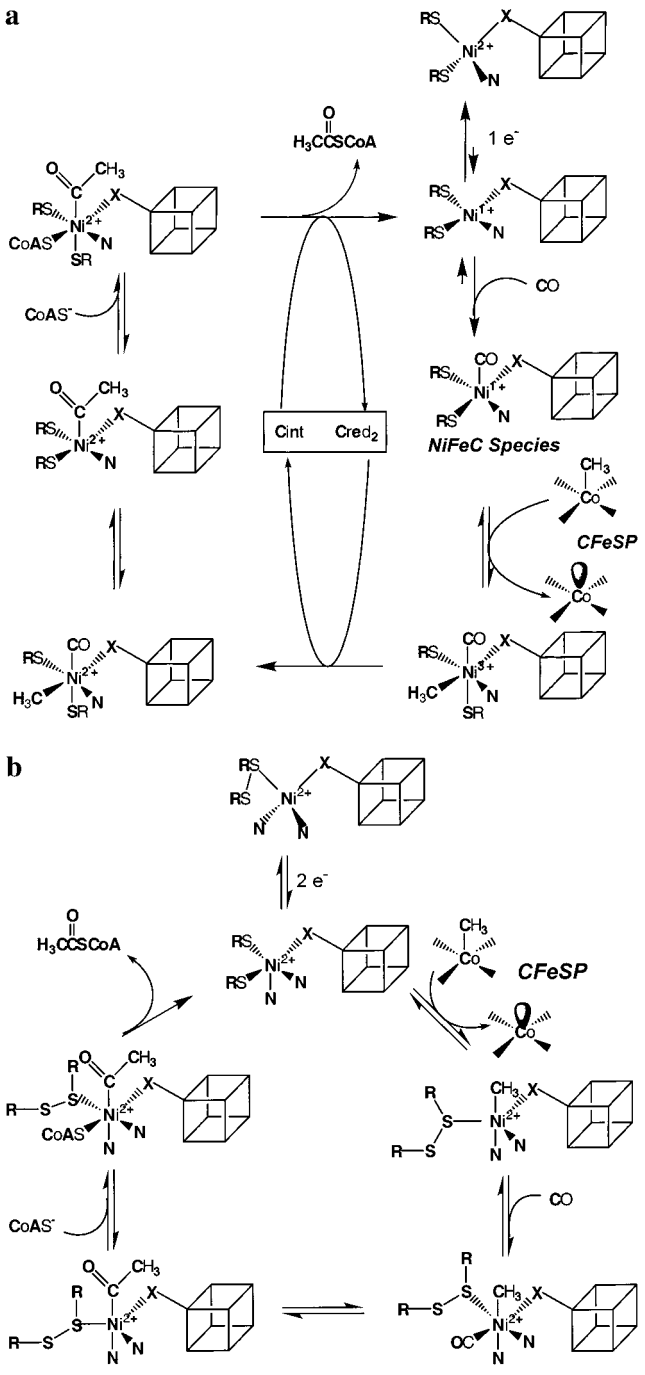

FIGURE 1: Scheme showing the paramagnetic (a) and diamagnetic (b) catalytic mechanisms of acetyl-CoA synthesis by CODH/ACS. C_{int} and C_{red2} are one-electron reduced and two-electron reduced forms of cluster C on the CODH subunit. Other abbreviations are as indicated in the text.

is not on the main catalytic route for acetyl-CoA synthesis (*29*) but is a nonfunctional side reaction (*28*). The loss of the EPR signal appears to conflict with the paramagnetic mechanism because the methyl group of the CH_3-CFeSP appears to be transferred in an S_N2 mechanism as a methyl cation to ACS (*10*, *11*, *30*, *31*). The reaction of a paramagnet (NiFeC species) with a diamagnetic methyl cation should yield another paramagnet. Furthermore, Lindahl et al. recently demonstrated that ACS activity is acutely inhibited by CO (*32*) and pointed out the rate of acetyl-CoA synthesis at optimal CO concentrations is significantly faster than the published rate of NiFeC species formation (0.12 s^{-1}) (*25*).

The most important criterion that a putative intermediate must meet is catalytic competence. To pass the test of catalytic competence, an intermediate must form and decay at kinetically relevant rates. The yardstick for kinetic relevance is the rate of the overall steady-state reaction. Explicitly defined for the NiFeC species, if it is a catalytically competent intermediate, it must form and decay at least as fast as the k_{cat} value of the steady-state reaction at saturating substrate concentrations and as fast as the value of k_{cat}/K_m times the substrate concentration at substrate concentrations below K_m. We have performed steady-state, stopped-flow, and rapid freeze-quench EPR studies to measure the rates of formation and decay of the NiFeC species and kinetic simulations to place the NiFeC intermediate in context of the overall steady-state reaction. Our results indicate that the NiFeC EPR signal represents a catalytically competent intermediate in acetyl-CoA synthesis. Our results support an S_N2-type displacement mechanism for methylation of CODH/ACS by the CH_3-CFeSP.

MATERIALS AND METHODS

Materials. CO (99.99%) and N_2 (99.998%) were purchased from Matheson Gas (Joliet, IL). N_2 (99.998%, Linde, Lincoln, NE) and other inert gases were purified from traces of oxygen by passage over a heated BASF catalyst. ^{14}C-Labeled methyl iodide was purchased from Pharmacia Amersham, while protocatechuic acid, methyl viologen, acetyl-CoA, and CoA were purchased from Sigma-Aldrich. Protocatechuic acid dioxygenase was a generous gift from Dr. David Ballou of the University of Michigan. Titanium trichloride ($TiCl_3$) was obtained from Pfalz and Bauer as a 30% w/v solution in 2.0 M HCl. All other chemicals were of analytical grade from Sigma-Aldrich and were used as purchased.

Growth of the Organism and Enzyme Purification. Moorella thermoacetica (formerly *Clostridium thermoaceticum* strain ATCC 39073) was grown with glucose as the carbon source at 55 °C as described (*33*). CODH/ACS was purified under strictly anaerobic conditions (*34*) in a Vacuum Atmospheres (Hawthorne, CA) anaerobic chamber maintained at 18 °C at an oxygen tension below 1 ppm. Oxygen levels were monitored continuously with a model 317 trace oxygen analyzer (Teledyne Analytical Instruments, City of Industry, CA). The CFeSP was purified as described (*35*). Both CODH/ACS and CFeSP were judged to be >95% pure by denaturing SDS−PAGE electrophoresis. Purified CODH/ACS had an average specific activity of 400−450 units/mg (1 unit = 1 μmol of CO oxidized/min) at 55 °C and pH 7.6 with 10 mM methyl viologen as electron acceptor (*34*). The average specific activity of CODH/ACS in the isotopic exchange reaction between CO and [1-^{14}C]acetyl-CoA was 200 nmol min^{-1} mg^{-1} at 55 °C using 200 μM acetyl-CoA, 0.57 mM CO, 0.1 M MES, pH = 6.0, and 0.1 mM methyl viologen. Protein concentrations were determined by the Rose Bengal method (*36*). Exchange assays at 25 °C were carried out in 0.1 M Tris-HCl, pH 7.60, in the absence of DTT, methyl viologen, CoA, and CH_3-CFeSP. Reactions were started with radiolabeled acetyl-CoA and contained 7.9 μM CODH/ACS and 0.28 mM unlabeled acetyl-CoA. The resulting exchange rate constants, measured at several CO concentrations, were plotted versus CO to obtain K_m and k_{cat} values. Variable CO concentrations were obtained by using premixed tanks containing 5%, 10%, 30%, 50%, and 100% CO and calculated by using a Henry constant of 0.98 mM/atm.

Methylation of the CFeSP. As-isolated CFeSP was freed of reductants by concentration and dilution with 0.1 M Tris-HCl, pH 7.60. For a typical methylation reaction, about 200 nmol of CFeSP was diluted to 4.0 mL, and 2.5 μmol of titanium citrate was added to reduced the Co^{2+} corrinoid to Co^{1+}. Reduction of the cobalt center was followed by measuring the UV−visible spectrum of a 20 μL aliquot of this solution diluted into 400 μL of 0.1 M Tris-HCl, pH 7.6, at room temperature using a Beckman DU7400 spectrophotometer. When reduction was nearly complete, 1.0 μmol of [^{14}C]CH_3I dissolved in neat methanol to a specific radioactivity of 12350 dpm/nmol of CH_3I was added to start the methylation reaction. The reaction was carried out at 55 °C for 10−15 min in the dark and monitored by UV−visible spectroscopy as described above. The reduced CFeSP exhibits a sharp absorbance with λ_{max} at 390 nm ($\epsilon_{390} = 40$ cm^{-1} mM^{-1}), and CH_3-CFeSP exhibits a broad absorption with λ_{max} at 450 nm ($\Delta\epsilon = 16.2$ OD mM^{-1} cm^{-1}). After completion of the reaction, CH_3-CFeSP was desalted three times with 0.1 M Tris-HCl, pH 7.60. The extent of methylation, quantified from the radioactivity of the sample, the protein concentration, and the absorbance at 450 nm, consistently yielded between 0.98 and 1.05 methyl groups/mol of monomeric CFeSP. CH_3-CFeSP for exchange assays was prepared using unlabeled CH_3I.

Steady-State Measurements. Reactions were carried out in semi-micro 1.7 mL cuvettes using a total reaction volume of 400 μL and at 25 °C in a Cary 14 spectrophotometer modified by OLIS, Inc. (Bogart, GA). Cuvettes were equilibrated with CO/N_2 gas mixtures at room temperature, the reaction mixture was added, and gases were bubbled into the solution. Then, CH_3-CFeSP was added, and its spectrum was recorded. The reaction was started by addition of CoA and CODH/ACS to give final concentrations of 0.5 mM and 0.54 μM, respectively, and monitored for ~10 min until completion at 390 and 450 nm. The initial slope of absorbance versus time was used to calculate initial rates (micromolar per minute) using extinction coefficients of 17.0 and 8.0 OD mM^{-1} cm^{-1} at 390 and 450 nm, respectively. In some experiments, samples were removed to measure the yield of acetyl-CoA by HPLC analysis as previously described (*37*). The concentration of acetyl-CoA was estimated by comparing the integration of the peak area with a calibration curve obtained using authentic acetyl-CoA.

CO/acetyl-CoA exchange assays were performed at 22 °C in the anaerobic chamber essentially as previously described (*38*) and started by adding [1-^{14}C]acetyl-CoA. The exchange assays contained 0.28 mM [1-^{14}C]acetyl-CoA (~1040 dpm/nmol), 1 atm of CO (980 μM CO), ~0.5 mM protocatechuic acid, protocatechuic acid dioxygenase (PCA), 0.1 M Tris, pH 7.60, and 7.9 μM ($\alpha\beta$ heterodimeric unit) CODH/ACS. The assays for inhibition of the CO/acetyl-CoA exchange by DTT or titanium citrate were performed with 0.2 mM acetyl-CoA. The temperature was maintained with a dry heat-block bath. A total of 10 aliquots of 40 μL each were taken at given time intervals and added to 40 μL of aerobic 0.1 M HCl to quench the reaction. The quenched samples were removed from the anaerobic chamber, scintillation cocktail was added (7 mL), and the ratioactivity remaining in the

samples was measured by liquid scintillation counting. The radioactivity (disintegrations per minute) was plotted versus time and fit to the exchange equation as previously described (*39*).

Stopped-Flow Studies. Stopped-flow experiments were carried on an Applied Photophysics spectrophotometer (SX.MV18) equipped with a photodiode array detector. Constant temperature was maintained with a bath of nitrogen-bubbled water from a circulating pump to maintain anaerobicity. Rigorous measures were taken to purge oxygen from the stopped-flow instrument. Solutions of enzymes and substrates were made in the anaerobic chamber in 0.1 M Tris-HCl, pH 7.60, containing 500 μM 3,4-dihydroxybenzoic acid (protocatechuic acid, PCA) and 1 unit/mL protocatechuic acid dioxygenase (PCD), which is henceforth referred to as PCA/PCD buffer. The solutions were then loaded into tonometers, which served as reservoirs for the drive syringes of the stopped-flow instrument. Gas mixtures containing 10%, 30%, and 100% CO (with balance nitrogen) were passed through an oxygen absorber (Oxyclear, Supelco) attached to a Schlenk gas line and connected to the tonometers whose gas phase was equilibrated with the solution for ~15 min before closing the upper two-way valve of the tonometer. The solutions were immediately transferred into the drive syringes of the stopped flow through Luer lock connectors and used within 30 min. The drive syringes were maintained anaerobically at 25 °C in a temperature-controlled bath of anaerobic water. The 160 mL volume of the tonometers is 40-fold higher than the total solution volumes employed (4 mL). Thus, the total pressure and the CO partial pressure are insignificantly affected by loading the solutions into the stopped-flow drive syringes. Since all reactants were diluted 2-fold during mixing, the final CO concentrations should be 50, 150, and 500 μM with 10%, 30%, and 100% CO, respectively. The methyl-transfer reaction from the CH_3-CFeSP to ACS was monitored in the single wavelength mode by following the decay in the CH_3-Co absorbance band at 450 nm and formation of the Co^{1+} peak at 390 nm. Reduction of the clusters of CODH/ACS and the CFeSP was monitored at 420 nm. The reactions were also followed with a photodiode array detector. A total of 400 scans were collected for 4 s using the program XScan and analyzed according to the program ProK, both from Applied Photophysics. Data were fitted to single- or double-exponential decay functions with software provided by Applied Photophysics (version SX MV.18). Reported rate constants are the average of at least five different rapid-mixing experiments.

RFQ Experiments. The rapid freeze-quench (RFQ) experiments followed the design described by Ballou (*40*) using a rapid-mixing apparatus from Update Instruments, Inc. (Madison, WI). Solutions of enzymes and substrates were prepared in PCA/PCD buffer as described in the previous section and loaded into the drive syringes. To add CO, 10 mL bottles containing the anaerobic solutions were capped with Subaseal septa (Aldrich catalog no. Z10075-7) in the chamber, equilibrated with 1 atm of the corresponding CO/N_2 gas mixture in the Schlenk line for 15 min, and moved into the anaerobic chamber. The solutions were then loaded into drive syringes by puncturing the stopper with a hose coupled to the syringe of the RFQ apparatus. The solution was pumped in and out several times with the plunger in order to ensure complete equilibration of the gas and solution phases and between the syringe and the CO-containing solution. The exact CO concentration was determined by removing a sample of the solution into a 1.0 cm path cuvette containing 1.0 mL of 10 mM methyl viologen, 2 mM DTT, and 50 mM Tris-HCl, pH 7.60, and ~1 μM CODH/ACS. The amount of CO dissolved in the solution was calculated from the total absorbance change at 604 nm after correction for dilution. Solutions lacking CO were loaded into the drive syringe in the anaerobic chamber under an atmosphere of nitrogen. The two syringes were connected to a mixer, which was connected in series to the reactor hose and the nozzle. To ensure anaerobicity, the reactor hose was washed and filled with PCA/PCD buffer inside the anaerobic chamber prior to each sample acquisition. For each data point, a total of four shots were collected, so the first pulse contained only PCA/PCD buffer. The reaction was stopped by spraying the solution into a funnel connected to an EPR tube, which was filled with liquid isopentane at −130 to −140 °C and immersed in a stirred bath of liquid isopentane. Adding liquid nitrogen as necessary controlled the bath temperature. Before each experiment was performed, the filling cup and the EPR tube were filled with liquid isopentane at room temperature and sparged with high-purity nitrogen gas for 15 min at −130 °C. The anaerobicity of the system was demonstrated by a control experiment in which CO-treated CODH/ACS was rapidly mixed with PCA/PCD buffer. The NiFeC signal, which is readily lost in the presence of traces of oxygen, was maintained over a period of 30 s. The intensity of the $g = 2.08$ derivative feature of the EPR spectrum of this control reaction was used as the zero time point for the experiment in which the decay of the signal was monitored. The RFQ samples were kept in liquid nitrogen prior to recording the EPR spectra at 77 K, within a few minutes after collecting and packing each sample. The conditions for recording the EPR are specified in the appropriate figure legends. The intensity of the EPR signal was measured directly from the spectra, plotted versus time, and fitted to a single-exponential equation.

EPR Spectroscopy. X-band EPR spectra were recorded in a Bruker ESP300e spectrometer connected to a Hewlett-Packard microwave frequency counter, model 5253B, and a Bruker gaussmeter, model ER 035. Samples were maintained in a Dewar filled with liquid nitrogen inside the EPR X-band cavity.

RESULTS

Steady-State Kinetic Studies of Acetyl-CoA Synthesis. To determine the catalytic relevance of a putative intermediate in an enzymatic reaction sequence, one must compare its rate of formation and decay with the steady-state rate of the reaction. For reactions involving CODH/ACS, this is complicated because there are complex relationships between rates and substrate concentrations. The steady-state rate of acetyl-CoA synthesis from CO, CoA, and CH_3-CFeSP (eq 2, above) can be measured by monitoring the decay of methyl-Co(III) at 450 nm or the formation of Co(I) at 390 nm (Figure 2A). This rate has been shown to depend linearly on the CH_3-CFeSP concentration (i.e., nonsaturable) at up to at least 0.20 mM (*41*). At 25 °C with 196 μM CO and 25 μM CH_3-CFeSP, the exponential fit of the time course yields a first-order rate constant of 0.0143 ± 0.0002 s^{-1}, which indicates a first-order dependence on [CH_3-CFeSP]. Thus

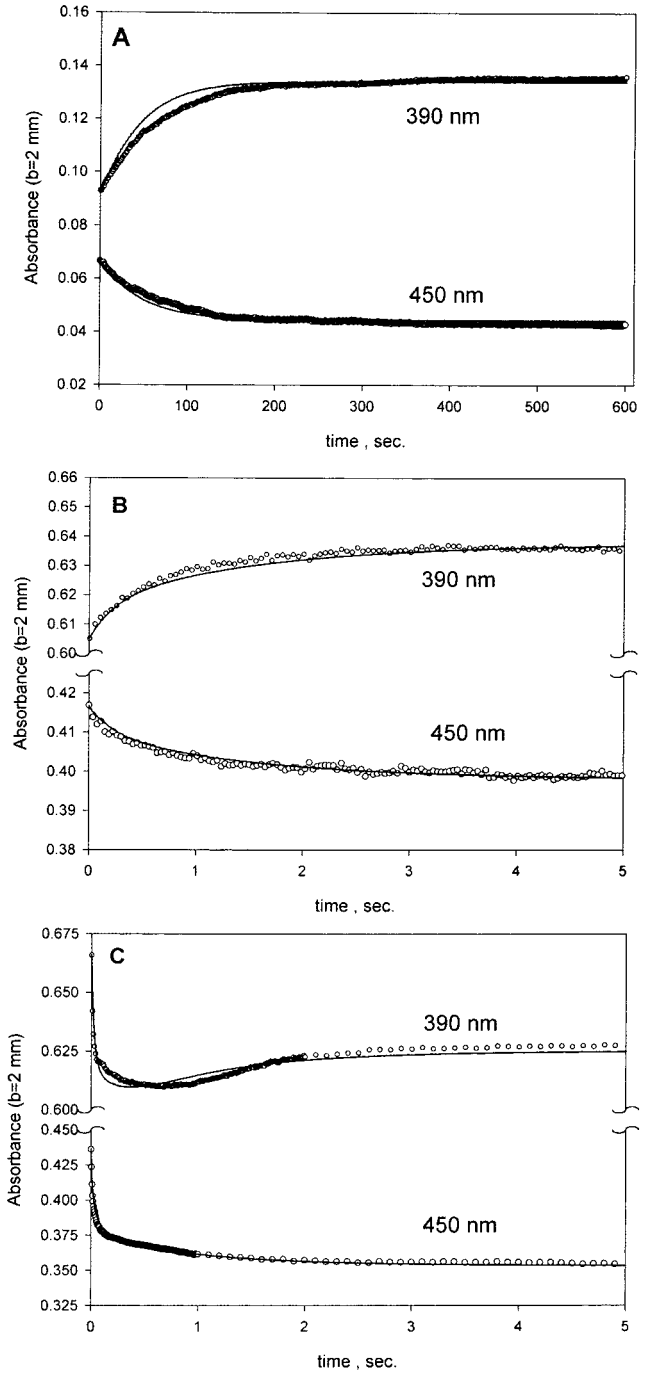

FIGURE 2: Steady-state and stopped-flow traces for the methyl transfer from CH_3-CFeSP to ACS. (A) Steady-state traces with 25 μM CH_3-CFeSP, 0.5 mM CoA, 196 μM CO, and 0.54 μM CODH/ACS, cell path = 2 mm. The single-exponential fits give k_{obs}, 0.0144 s^{-1}; amplitude, 0.0421 at 390 nm; k_{obs}, 0.0143 s^{-1}; amplitude, −0.0227 at 450 nm. (B) 43.5 μM CH_3-CFeSP, 0.5 mM CoA, 150 μM CO, and 50 μM CODH/ACS. CODH/ACS premixed with CoA and 30% CO. Triple-exponential fits of the traces yielded k_{obs} values of 83.8, 2.43, and 1.02 s^{-1} and amplitudes of −0.0426, −0.0567, and +0.0611 at 390 nm, respectively. At 450 nm, the rate constants are 83.7, 10.3, and 0.89 s^{-1} with amplitudes of −0.0464, −0.0264, and −0.0295, respectively. (C) 50 μM CH_3-CFeSP, 0.5 mM CoA, 150 μM CO, and 50 μM CODH/ACS. CODH/ACS premixed with CH_3-CFeSP versus CoA and CO (30%). Other conditions are 25 °C, 0.1 M Tris-HCl, pH 7.60, 500 μM 3,4-dihydroxybenzoic acid, and protocatechuic acid dioxygenase. Single-exponential fits give k_{obs} of 1.21 s^{-1} with an amplitude of +0.0281 at 390 nm and k_{obs} of 1.27 s^{-1} with an amplitude of −0.0142 at 450 nm. Note that the solid lines are not the fits but simulations with the mechanism shown in Scheme 1 and rate constants shown in Table 3.

the second-order rate constant (with respect to CH_3-CFeSP) is 26000 M^{-1} s^{-1}. The thin solid lines shown are simulations of the steady-state reaction using rate constants and the mechanism derived from the rapid kinetics experiments described below.

Although CO is a saturable substrate for the acetyl-CoA synthesis reaction, it is also a potent substrate inhibitor exhibiting highly cooperative behavior (*32*). At 1 atm of CO (980 μM in solution), with 50 μM CH_3-CFeSP at 25 °C and pH 7.6, we measured a steady-state rate constant (vel/[ACS]) of 0.17 s^{-1} (data not shown), in agreement with previous reports (*19*, *32*, *37*, *42*). Decreasing the CO concentration to 196, 98, and 49 μM increases the rate constant to 0.32 ± 0.06, 1.2 ± 0.1, and 1.45 ± 0.35 s^{-1}, respectively. These results agree with those of Maynard et al. (*32*) that the K_m for CO in acetyl-CoA synthesis is below 100 μM and that higher concentrations than 100 μM are inhibitory. From their results, the acetyl-CoA synthesis rate at 0.1 mM CO is predicted to be 90% of the value at 0.1 mM, yielding a rate constant of 1.0 s^{-1}.

Interestingly, the inhibitory behavior by CO observed in acetyl-CoA synthesis is not exhibited in the isotope-exchange reaction between free unlabeled CO and the labeled carbonyl group of acetyl-CoA (Figure 1 in Supporting Information). In this reaction, as soon as the C−C and C−S bonds of acetyl-CoA are cleaved and CO, the methyl group, and CoA are bound to CODH/ACS, the bound carbonyl group can equilibrate with free CO. The exchange rate shows a hyperbolic dependence on CO concentration, with Michaelis−Menten parameters of V_{max} = 107 ± 32 μM min^{-1} (k_{cat} =0.23 s^{-1}) and K_m(CO) = 990 ± 500 μM. This relatively high standard error is because a solution saturated with 1 atm of CO is 980 μM. At 110 μM CO, the exchange rate is 0.05 s^{-1} (see Figure 1 in Supporting Information). DTT and titanium citrate (2 mM) inhibit the exchange activity by 10-fold (Figure 2 in Supporting Information). The importance of the effect of these reagents on the exchange assay will become apparent in the discussion of their effect on the NiFeC species.

In summary, the complex behavior of CODH/ACS with respect to its substrates observed in steady-state experiments indicates that rapid kinetics experiments should be performed under analogous conditions. Conclusions regarding the catalytic competence of any putative intermediate should include a comparison of such analogous reactions.

Some Experimental Concerns Related to Performing Rapid Kinetics Studies on CODH/ACS. Rapid kinetics studies are performed at high enzyme concentrations, which presents an experimental problem because, using CO concentrations below 0.1 mM, where it does not inhibit acetyl-CoA synthesis (above), the CO concentration becomes nearly equivalent to that of CODH/ACS. Then, it becomes difficult to accurately control the CO concentration because some of the CO is depleted to reductively activate the enzyme. Because of these complications, we measure the amount of CO in solution in each set of experiments. Another experimental complication that limits our choice of mixing conditions in the rapid kinetics experiments is that preincubation of the CH_3-CFeSP with CoA leads to demethylation of the methyl corrinoid. The thiol-dependent demethylation of methyl corrinoids has been studied by Hogenkamp (*43*).

Several chromophoric prosthetic groups are present in the rapid kinetics experiments described below that can undergo reduction upon reaction with CO, including the FeS clusters on CODH/ACS (clusters A, B, C, and D) and the cobamide and the $[Fe_4S_4]$ cluster of the CFeSP. The CODH/ACS-catalyzed reduction of Co^{2+}-CFeSP by CO appears to be independent of CO at concentrations between 49 and 980 μM but linearly dependent on the CFeSP concentration, with a second-order rate constant at 25 °C of 20000 M^{-1} s^{-1} (data not shown). This is in agreement with the previously determined rate constant of ~60000 M^{-1} s^{-1} at 55 °C (*41*). Thus, with 50 μM CFeSP, Co^{2+} reduction to Co^{1+} occurs with k_{obs} of 1 s^{-1}. Reduction of the $[Fe_4S_4]^{2+}$ cluster of the CH_3-CFeSP to $[Fe_4S_4]^{1+}$ by CO and CODH/ACS, which is monitored by following bleaching of the $[Fe_4S_4]^{2+}$ absorption band at 420 nm, occurs with a second-order rate constant of 30000 M^{-1} s^{-1} at 25 °C and also is linear with respect to CH_3-CFeSP concentration (data not shown). Therefore, reduction of $Co^{2+}$and the $[Fe_4S_4]^{2+}$ cluster of the CFeSP and of the synthesis of acetyl-CoA occurs at approximately the same rate, and all display first-order dependence on the corrinoid protein substrates.

RFQ EPR Experiments. To probe the participation of the paramagnetic NiFeC species in the synthesis of acetyl-CoA, we followed the decay and formation of the NiFeC EPR signal by RFQ experiments using conditions similar to those of the steady-state experiments described above.

To follow decay of the NiFeC species, CO-preincubated CODH/ACS is reacted with the other substrates required for acetyl-CoA synthesis (eq 3). When a solution containing 100 μM CODH/ACS, 1 mM CoA, and 30% CO (0.12 mM final, measured after mixing) is rapidly mixed with 100 μM CH_3-CFeSP, the NiFeC EPR signal decays with an apparent rate constant of 6 s^{-1} (Figure 3). The signal does not decay completely; instead, 33% of its initial intensity remains at the end of the reaction. This indicates that either the signal decays and then re-forms during a later cycle of catalysis or that the decay is reversible. A 33% final intensity would be consistent with a re-formation rate constant of about 1−2 s^{-1} coupled to a decay of 6 s^{-1}. The decay rate constant is significantly larger than the steady-state rate constant for acetyl-CoA synthesis (1.1 s^{-1} at 98 μM CO and 0.65 s^{-1} at 196 μM CO), which demonstrates that the paramagnetic NiFeC species meets this measure of catalytic competence as an intermediate in the acetyl-CoA synthesis reaction.

$$[\text{CODH/ACS}][\text{CO}][\text{CoA}] + \text{CH}_3\text{-CFeSP} \rightarrow \text{acetyl-CoA} + \text{CFeSP} + \text{CODH/ACS (decay mode)} \quad (3)$$

$$[\text{CODH/ACS}][\text{CH}_3\text{-CFeSP}] + \text{CO} + \text{CoA} \rightarrow \text{acetyl-CoA} + \text{CFeSP} + \text{CODH/ACS (formation mode)} \quad (4)$$

Although the NiFeC decay rate meets the criterion of catalytic relevance, it is equally important to test the rate at which the NiFeC species forms. We have followed the rate of NiFeC species formation by preincubating CODH/ACS with the methylated CFeSP and reacting this mixture with CO under conditions similar to the steady-state acetyl-CoA synthesis reaction (eq 4). When a solution containing 100 μM CODH/ACS and 100 μM CH_3-CFeSP is rapidly mixed with 1 mM CoA and 30% CO (0.12 mM final measured concentration), the EPR signal forms with a k_{obs} of 0.9 s^{-1} (Table 1 and Figure 4). Thus, within experimental error, the rate of formation of the NiFeC EPR signal occurs at the same rate as acetyl-CoA synthesis under steady-state conditions, which is approximately 1.0 s^{-1} at 0.12 mM CO (see steady-state section, above). These results indicate that the NiFeC signal is an intermediate in acetyl-CoA synthesis and its formation is almost fully rate-limiting in the overall reaction.

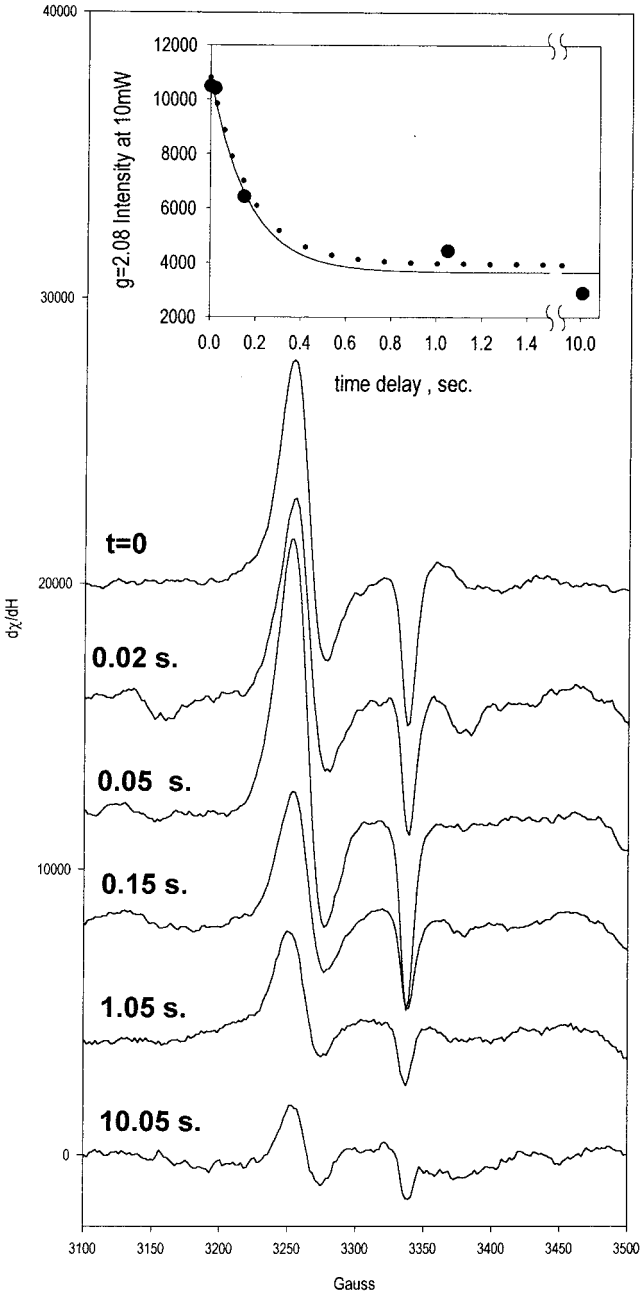

FIGURE 3: RFQ of 100 μM CODH/ACS, 1.0 mM CoA, and 30% CO versus 100 μM CH_3-CFeSP. Other conditions were 0.1 M Tris-HCl, pH 7.60, 500 μM 3,4-dihydroxybenzoic acid, and protocatechuic acid dioxygenase. EPR spectra were recorded at the following conditions: *T*, 77 K; microwave frequency, 9.467 GHz; microwave power, 10 mW; gain, 20000; modulation frequency, 100 kHz; modulation amplitude, 10.14 G. The inset shows the decay of the $g = 2.08$ feature of the NiFeC species, with the parameters as indicated in Table 1. The dotted line is a simulation to the mechanism shown in Scheme 1 and with rate constants shown in Table 3.

Table 1: Stopped-Flow and RFQ Experiments Using 110−130 μM CO[a]

first syringe	CODH/ACS, CO, CoA	CODH/ACS, CoA	CODH/ACS, CH_3-CFeSP
second syringe	CH_3-CFeSP	CO, CH_3-CFeSP	CO, CoA
stopped flow	decay mode	decay mode	formation mode
k_{obs} (s^{-1})	1.17 ± 0.07	0.49 ± 0.1	1.4 ± 0.3
amplitude (μM)	7.9 ± 0.2	25 ± 8	13.9 ± 0.7
RFQ	NiFeC decay	NiFeC formation	NiFeC formation
k_{obs} (s^{-1})	6.0 ± 2		0.86 ± 0.11
amplitude	7150 ± 900[b]		19600 ± 700[c]
offset	3600 ± 600[b]		0

[a] Other conditions are 110−130 μM CO, 50 μM CH_3-CFeSP, 50 μM CODH/ACS, 0.5 mM CoA, and 0.1 M Tris-HCl, pH 7.60, ~22 °C. [b] EPR spectra recorded at 80 K; power, 10 mW; gain, 20000; modulation frequency, 100 kHz; modulation amplitude, 10 G. [c] EPR spectra were recorded at 80 K; power, 40 mW; gain, 20000; modulation frequency, 100 kHz; modulation amplitude, 10 G.

We also studied the rate of NiFeC species formation in the absence of CH_3-CFeSP and CoA by mixing CODH/ACS with CO in a RFQ experiment and obtained a formation rate constant of 0.7 ± 0.2 s^{-1}. This indicates that neither the methylated CFeSP nor CoA significantly affects the rate of NiFeC species formation. However, these rate constants of ~1 s^{-1} are significantly larger than the value of 0.1 s^{-1} measured in earlier RFQ studies, when CODH/ACS was rapidly mixed with CO in the absence of CH_3-CFeSP and CoA but in the presence of DTT (*25*). When 2 mM DTT is added to the RFQ reaction of CODH/ACS with CO (in the presence of absence of CoA), as before, we obtain a rate constant of ~0.1 s^{-1}. Thus, DTT markedly inhibits formation of the NiFeC species, which is consistent with the 4.5-fold reduction observed in CO/acetyl-CoA exchange rates by 2 mM DTT (above). Since the binding of CO to cluster A, which elicits the NiFeC paramagnetic state, presumably does not compete with CH_3-CFeSP, it is likely that CO is the first substrate binding to ACS during acetyl-CoA synthesis.

The final intensity of the NiFeC signal formed in the RFQ experiment is ~7 μM (0.14 spin per $\alpha\beta$ heterodimer). For the RFQ experiment in which the decay of the NiFeC signal is monitored, the intensity of the EPR signal decays to 33% of the initial intensity, corresponding to ~4 μM concentration. In contrast, the same preparation of CODH/ACS equilibrated with an atmosphere of 100% CO, without either CoA or CH_3-CFeSP, yields 0.25 spin of NiFeC per CODH/ACS. To explain the difference in final intensities and concentrations, the NiFeC species must be in equilibrium with another active form(s) of the A-cluster of ACS during acetyl-CoA synthesis, indicating that this species is in flux, forming and decaying during the overall reaction. Therefore, when all of the substrates for acetyl-CoA synthesis are present, the formation and decay of the NiFeC species must *not* correspond to a single-step process, i.e., binding and release of CO. Kinetic simulations were carried out to further support the argument that the formation and decay are serial steps in the mechanism of acetyl-CoA synthesis.

Stopped-Flow Studies of Methyl Transfer from CH_3-CFeSP to CODH/ACS. (A) Reaction of CH_3-CFeSP with CODH/ACS, CO, and CoA. We previously followed acetyl-CoA synthesis from CH_3-CFeSP, CO-preincubated CODH/ACS, and CoA by stopped-flow kinetics (*44*). These earlier

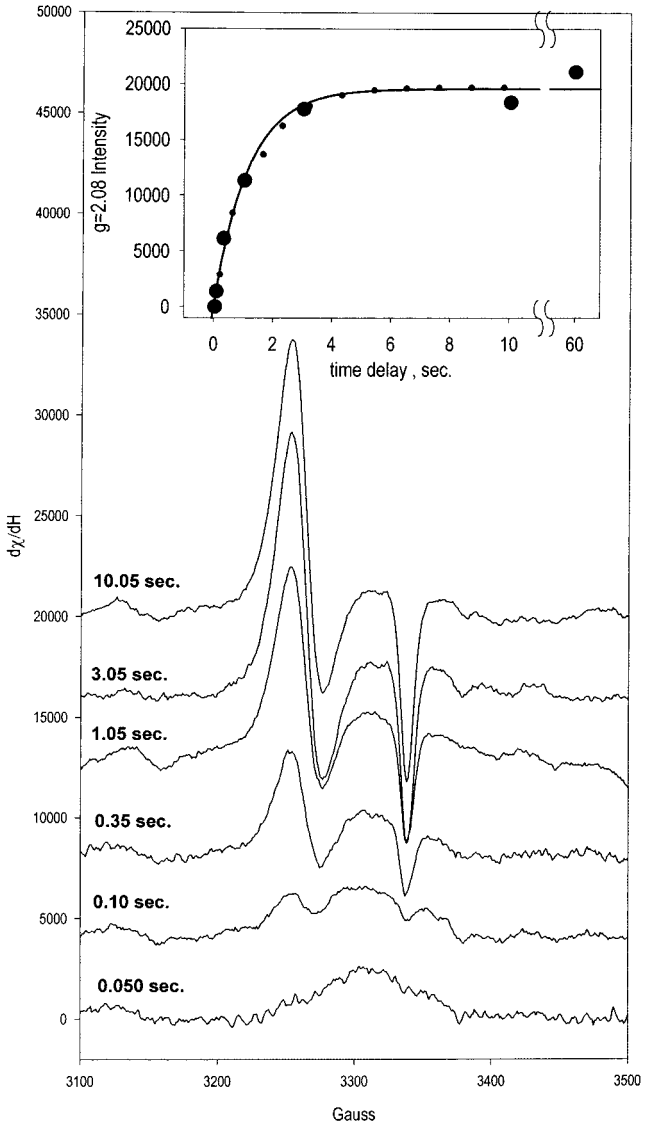

FIGURE 4: RFQ of 100 μM CODH/ACS and 100 μM CH_3-CFeSP versus 240 μM CO and 1.0 mM CoA. Other conditions are 0.1 M Tris-HCl, pH 7.60, 500 μM 3,4-dihydroxybenzoic acid, and protocatechuic acid dioxygenase. EPR spectra were recorded at the following conditions: *T*, 77 K; microwave frequency, 9.467 GHz; microwave power, 40 mW; gain, 20000; modulation frequency, 100 kHz; modulation amplitude, 10.14 G. The inset shows the dependence of the $g = 2.08$ feature of the NiFeC species with time. Parameters are shown in Table 1. The dotted line is a simulation to the mechanism outlined in Scheme 1 and with the rate constants from Table 3.

experiments demonstrate that the absorbance at 390 nm increases as Co^{1+} is formed, that the 450 nm absorbance band decreases as CH_3-Co^{3+} decays, and that clean isosbestic points at the expected wavelengths are observed. We have repeated these stopped-flow experiments under conditions similar to those of the steady-state and RFQ experiments monitoring NiFeC signal decay (above and depicted in eq 3). Here we monitored the reaction by rapid-scanning photodiode array spectroscopy (Figure 2C). The major spectral changes can be assigned to conversion of CH_3-Co^{3+} of the methylated CFeSP to the Co^{1+} state with a single-exponential ($k_{obs} = 1.2$ s^{-1}) decrease in absorbance at 450 nm and a corresponding single-exponential increase at 390 nm. This rate constant is similar to that observed for the steady-state formation of acetyl-CoA (above). These results

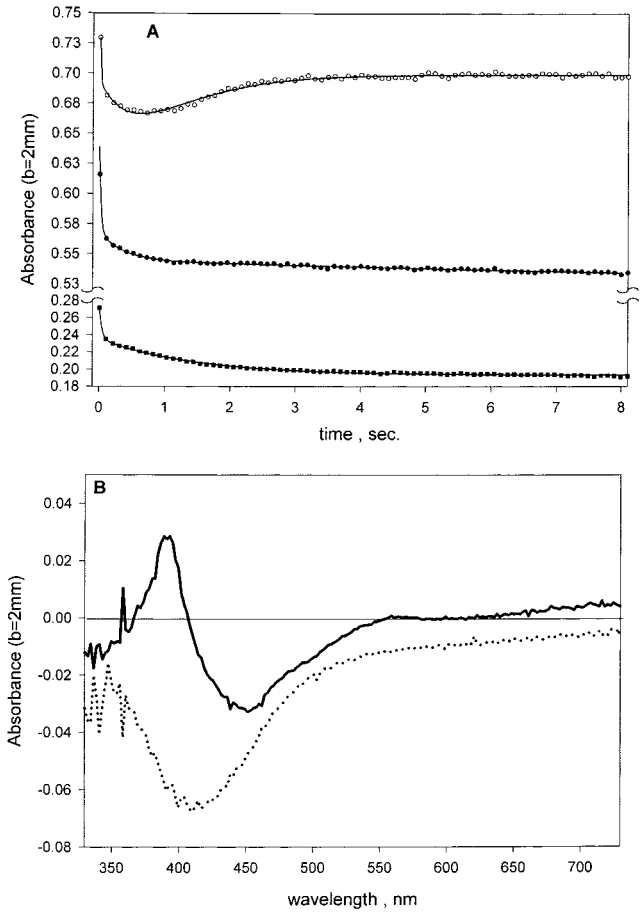

FIGURE 5: (A) Stopped-flow experiments following the demethylation of CH_3-CFeSP at 390 nm (top), 420 nm (middle), and 450 nm (bottom). In these experiments, 100 μM CODH/ACS and 100 μM CH_3-CFeSP were rapidly mixed with 1 mM CoA and 30% CO at 25 °C. Other conditions are 0.1 M Tris-HCl, pH 7.60, 500 μM protocatechuic acid, and protocatechuic acid dioxygenase. (B) Difference spectra at two time intervals. The solid line shows the formation of Co^{1+}-CFeSP at 390 nm concomitant with decay of CH_3-Co^{3+}-CFeSP at 450 nm, obtained by subtracting the spectrum at 0.52 s from the spectrum at 8.0 s. The dotted line shows the bleaching of $[Fe_4S_4]$ clusters, and it was obtained by subtracting the spectrum at 0.009 s from the spectrum at 0.52 s.

are consistent with a process lacking an intermediate (e.g., CH_3-Co^{2+}, Co^{2+}). Since CODH/ACS was preincubated with CO, the $[Fe_4S_4]$ clusters of CODH/ACS were initially in the B_{red} and C_{red2} states, and no net change in their redox state was observed during these experiments.

(B) Reaction of CH_3-CFeSP and CODH/ACS with CO and CoA. To measure the kinetics under the same conditions as in the RFQ experiments monitoring formation of the NiFeC species, a solution containing CODH/ACS and the CH_3-CFeSP was reacted with 145 μM CO and 0.5 mM CoA in the rapid-scanning stopped-flow apparatus. In contrast to the decay experiment, three exponential phases are observed at 390 and 450 nm during the 5 s reaction (Figure 2B and Figure 5). The first two exponentials observed during the first 400 ms have rate constants of 100 and 10 s^{-1} and exhibit decreases in absorbance at both 450 and 390 nm. The difference spectrum shown in Figure 5A indicates that the spectral changes result from $[Fe_4S_4]^{2+}$ cluster reduction. These rate constants are similar to the rates of $[Fe_4S_4]^{2+}$ cluster reduction observed previously at 420 nm when CODH/ACS was reacted with 145 μM CO (final concentration), without CoA or CH_3-CFeSP (*45*). These results indicate that the first two exponential changes correspond to reduction of two of the $[Fe_4S_4]^{2+}$ cubanes in CODH/ACS. We assign the first decay to reduction of the B-cluster of CODH and the second one to the reduction of nonlabile Ni-containing $[Fe_4S_4]^{+2}$ clusters. The rationale for this assignment is covered in the Discussion section. The reduction of the B- and C-clusters by CO occurs much faster than the synthesis of acetyl-CoA (*25*, *45*). The conversion of C_{red1} to C_{red2} does not involve changes in the UV−visible spectrum of CODH (*46*), since both species contain a $[Fe_4S_4]^{1+}$ cluster (*47*) and occurs at a even faster rate than the reduction of the B-cluster (*45*).

In contrast to the first two exponential phases just described, where the absorbances at 390 and 450 nm both decrease, in the third exponential phase, observed between 0.4 and 4 s in Figure 5A, the absorbance at 390 nm increases as that at 450 nm decreases. The difference spectrum (Figure 5B) clearly shows that the third exponential phase of the stopped-flow experiment results from methyl transfer from methylated CFeSP to ACS, as CH_3-Co^{3+} is converted to Co^{1+}. The rate constant for the third exponential phase (k_{obs} $\sim$ 1.0 s^{-1}) matches the single-exponential rate constant for the RFQ experiment in which NiFeC species formation was monitored. It also matches the steady-state k_{cat} for acetyl-CoA synthesis (above). These combined results suggest that the methyl-transfer reaction associated with the third exponential phase is rate-limited by the formation of the NiFeC species.

Further Studies of the Reaction of CH_3-CFeSP with CODH/ACS, CO, and CoA. In the stopped-flow experiments performed under conditions similar to those of the RFQ decay experiments, the rate constant was only 1 s^{-1}, whereas decay of the NiFeC signal occurs with a rate constant of 6 s^{-1}. Since CO inhibits the steady-state rate of acetyl-CoA synthesis, we wondered if CO inhibition might explain this lower than expected rate constant. We decreased the CO concentration in the preincubation mixture. When a solution containing CODH/ACS, CoA, and 98 μM CO is reacted with 50 μM CH_3-CFeSP, two exponential changes are observed at both 390 and 450 nm with rate constants of 30 and 2 s^{-1} (Figure 6). Since the enzyme is preincubated with reductant (CO), $[Fe_4S_4]^{2+}$ reduction is not observed as in the stopped-flow traces shown in Figure 2C; instead, both phases reflect the transmethylation reaction, conversion of CH_3-Co^{3+} to the Co^{1+} form of the CFeSP. The rate constant for the first exponential phase is about 15-fold higher than the steady-state rate of acetyl-CoA synthesis, and its amplitude corresponds to 0.14 methyl group transferred per ACS. This result could be due to either an unfavorable equilibrium for methyl group transfer from CH_3-CFeSP to ACS or to only ~14% of the ACS molecules bearing active methyl-accepting sites. We favor the second explanation because the amplitude of the pre-steady-state phase in the stopped-flow experiment is similar to the amount of NiFeC signal. The amount of A-clusters that can be methylated also equals the amount of labile Ni present in CODH/ACS [defined as the amount of Ni that can be removed by *o*-phenanthroline (*23*, *48*)] and the amount of CoA that can bind to ACS (*27*). Thus, the concentration of active ACS is 4−5-fold less than the concentration of CH_3-CFeSP, allowing for multiple turnovers of active ACS.

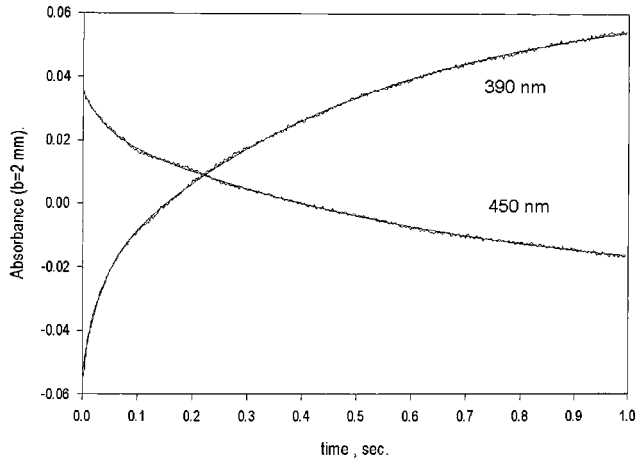

FIGURE 6: Example of stopped-flow traces for the demethylation of CH_3-CFeSP at two wavelengths. 100 μM CODH/ACS, 98 μM CO, and 1 mM CoA were rapidly mixed with 100 μM CH_3-CFeSP at 25 °C in 0.1 M Tris-HCl, pH 7.60. The line for the 450 nm trace (decrease) corresponds to a double-exponential fit with the following parameters: amplitude$_1$ = −0.0117, k_1 = 24.6 s^{-1}; amplitude$_2$ = −0.0505, k_2 = 1.56 s^{-1}. The trace at 390 nm (increase) was also fitted to a double-exponential function with the following parameters: amplitude$_1$ = +0.0296, k_1 = 21.5 s^{-1}; amplitude$_2$ = +0.0894, k_2 = 2.04 s^{-1}.

Table 2: Rate Constants from Stopped Flow and Steady State: Experiments of Methyl Transfer from CH_3-CFeSP to CODH/ACS[a]

	stopped flow	
	49 μM CO	490 μM CO
first phase		
k_{obs} (s^{-1})	31 ± 5	
amplitude (μM)	7.5 ± 1.7	
second phase		
k_{obs} (s^{-1})	2.0 ± 0.2	2.5 ± 0.3
amplitude (μM)	29 ± 3	7.4 ± 1.2
steady state[b]		
vel/[Et] (s^{-1})	1.20 ± 0.12	0.43 ± 0.05
amplitude (μM)	21.5 ± 3.5	12.6 ± 0.3

[a] Other conditions are 50 μM CODH/ACS, CH_3-CFeSP, 0.5 mM CoA, and 0.1 M Tris-HCl, pH 7.60, ~22 °C. All experiments were started with rapidly mixing CODH/ACS, CO, and CoA versus CH_3-CFeSP. [b] Steady-state kinetics were measured at 390 and 450 nm at 25 °C with concentrations identical to those in footnote *a* except that the CODH/ACS concentration was 0.37 μM.

Since the concentration of CH_3-CFeSP is much greater than that of active ACS, we assign the second exponential in this decay experiment (Figure 6) to the steady-state reaction on the basis of the following arguments. First, the steady-state rate constant with 49 μM CO is similar (vel/[CODH/ACS] = 1.2 s^{-1}) to the average rate constant for the second exponential (2.0 s^{-1}). Second, the exponential behavior for this phase is diagnostic of first-order kinetics, which is expected since the steady-state rates are linearly dependent on the concentration of CH_3-CFeSP (*41*). Third, the amplitude of the second exponential is 29 ± 3 μM (Table 2), which corresponds to about 56% turnover of the CH_3-CFeSP. This is similar to the extent of demethylation observed in steady-state experiments with catalytic CODH/ACS (0.54 μM).

When a solution containing CODH/ACS, 1 mM CoA, and 980 μM CO is rapidly mixed with CH_3-CFeSP, a single-exponential phase is observed at 390 and 450 nm (Table 2), with an amplitude of 7.4 μM and a rate constant of 2.2 ± 0.3 s^{-1}. Since this rate constant is only about ~4-fold faster than the observed steady-state rate, it implies that as the CO concentration is increased above ~50 μM CO, the rate of methyl transfer is inhibited by CO to the point of becoming partially rate-limiting for acetyl-CoA synthesis. Therefore, CO appears to inhibit the steady-state acetyl-CoA synthesis reaction by preventing productive methylation of ACS.

DISCUSSION

CODH/ACS plays a central role in the Wood−Ljungdahl pathway (*4*, *38*). A number of important questions remain about how CODH/ACS accomplishes the final steps in this pathway, which include the condensation of a methyl group from CH_3-CFeSP with CO and CoA to form acetyl-CoA. We have presented evidence favoring a "paramagnetic" mechanism rather than a "diamagnetic" mechanism. The key distinction between these mechanisms relates to whether the paramagnetic NiFeC species is a catalytically relevant intermediate in acetyl-CoA synthesis. Can we rule out the intermediacy of this NiFeC species? What is the preferred order in which the three substrates bind to the enzyme, or do they bind randomly? What are the rate constants for the elementary steps in acetyl-CoA synthesis? CO is a potent substrate inhibitor (*32*). Which step in the overall reaction is subject to CO inhibition? We have performed rapid-mixing and steady-state kinetic experiments to address these questions.

Catalytic Competence of the Paramagnetic NiFeC Species? As described in the introduction, a number of experiments have been performed that support, and a few that appear to oppose, the catalytic intermediacy of the paramagnetic NiFeC species. We have attempted to gain evidence favoring or negating the paramagnetic mechanism by testing the hypothesis that the paramagnetic NiFeC species is an intermediate in acetyl-CoA synthesis. The NiFeC species exhibits a well-characterized EPR signal. If the rate of formation or decay of the NiFeC EPR signal is significantly slower than the steady-state rate of acetyl-CoA synthesis, we can rule out the paramagnetic mechanism.

The results of RFQ experiments strongly support the catalytic competence of the paramagnetic NiFeC species. When CODH/ACS and CO are rapidly mixed under non-inhibitory CO concentrations, the rate of NiFeC EPR signal formation (0.9 s^{-1} at 0.12 mM CO and 25 °C) matches the steady-state rate of acetyl-CoA synthesis. In addition, when CODH/ACS is preincubated with CoA and CO to preform the NiFeC signal and then is rapidly mixed with CH_3-CFeSP, the rate at which the NiFeC signal decays (6 s^{-1}) is significantly faster than the steady-state rate of acetyl-CoA synthesis. These results provide strong support for the catalytic competence of the NiFeC species: both decay and formation of the NiFeC EPR signal occur at rates that are consistent with the steady-state rate of acetyl-CoA synthesis.

The rate of NiFeC signal formation measured here (0.9 s^{-1}) is significantly faster than that measured in earlier studies (0.1 s^{-1}) and here, under certain conditions (*25*). This is important because it was recently shown that CO is a potent substrate inhibitor and that the rate of acetyl-CoA synthesis at 0.1 mM CO is ~10-fold faster than at 1 mM (*32*). Therefore, a formation rate constant of only 0.1 s^{-1} was considered as evidence contradicting the intermediacy of the

paramagnetic NiFeC species and supporting the diamagnetic mechanism (*32*). But since the rate of NiFeC EPR signal formation was similar to the rates of acetyl-CoA synthesis and the CO/acetyl-CoA exchange reaction, when performed under the same conditions, including the same CO concentrations, it could have been reasonably argued that those studies also supported the "paramagnetic cycle". Given that CO concentrations above 0.1 mM have no effect on the rate of formation of the NiFeC species, the earlier studies also support the paramagnetic mechanism outlined in Figure 1.

The RFQ studies and the results of the CO/acetyl-CoA exchange reaction described here demonstrate that the rate constants measured earlier were lower because the reactions were performed in the presence of relatively high concentrations of 2 mM DTT. The origin of this inhibition could be a direct interaction of the sulfur atoms of DTT with Ni^{2+} of cluster A, since DTT protects ACS toward removal of Ni^{2+} by the chelator *o*-phenanthroline (*48*). Alternatively, DTT could invoke a redox-dependent conformational change, since DTT does not affect the extent of NiFeC signal that is observable when ACS is equilibrated with CO. Although CoA affects the morphology of the NiFeC EPR signal (*16*), it does not appear to affect its rate of formation.

Another argument supporting the catalytic intermediacy of the NiFeC species is that the observed rate of NiFeC EPR signal decay is similar to the rate of methyl transfer, measured by following Co^{1+} formation in the stopped flow. This indicates that methyl transfer and decay of the paramagnetic intermediate occur during the same step. This is inconsistent with the diamagnetic mechanism, which represents the paramagnetic NiFeC species as a dead-end state (*23*). The diamagnetic mechanism would require that ACS must undergo oxidation (to produce diamagnetic Ni^{2+}) at a much faster rate than the subsequent methyl-transfer step before it can enter the catalytic cycle. Since the fraction of active ACS sites is identical to the ACS fraction that gives rise to the NiFeC signal, a scheme in which the decay of the NiFeC complex and methyl transfer are parallel reactions occurring at two different ACS molecules can also be ruled out. In contrast, the rate of NiFeC decay equals the methyl-transfer rate, which is inconsistent with the diamagnetic mechanism and consistent with the paramagnetic mechanism. As proposed, with methylation preceding CO binding (*23*), CO must also be released before ACS can undergo methylation, requiring another very rapid step before the methyl transfer. However, we do not view this to be a cardinal requirement of the diamagnetic mechanism; i.e., the order of binding could be first CO and then methyl, as we propose for the paramagnetic mechanism.

Another argument supporting the catalytic relevance of the NiFeC species is that this species is accommodated within a kinetic scheme that is consistent with the rapid-mixing and steady-state kinetic data presented above. We simulated the stopped-flow, steady-state, and RFQ traces with the program KINSIM (*49*); then, using FITSIM (*49*), we fitted the kinetic traces to obtain values for the individual rate constants. The kinetic mechanism used in the fits is shown in Scheme 1, which is a kinetic formulation of Figure 1a. The rate constants obtained from this analysis are given in Table 3, and the simulations of the stopped-flow (Figure 2), RFQ (Figures 3 and 4), and the steady-state (Figure 2) data according to this scheme fit the data quite well.

Scheme 1[a]

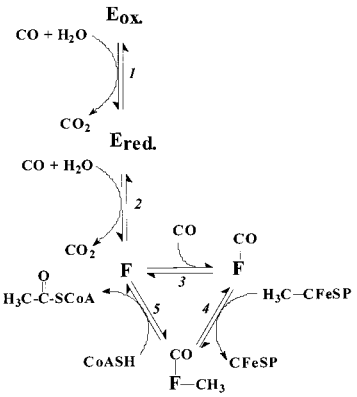

[a] Notation: E_{ox}, CODH/ACS with oxidized B-cluster; E_{red}, CODH/ACS with reduced B-cluster; F, CODH/ACS with both B- and $[Fe_4S_4]_A$-clusters reduced; F−CO, carbonylated NiFeC intermediate species; F−CO−CH_3, ternary methyl-CO−CODH/ACS complex (diamagnetic). This complex is kinetically indistinguishable from an acetyl-CODH/ACS complex.

Table 3: Summary of Rate Constants for Individual Steps of Acetyl-CoA Synthesis[a]

Scheme 1 step no.	k_{on} ($\mu M^{-1} s^{-1}$) (forward direction)	k_{off} ($\mu M^{-1} s^{-1}$) (reverse direction)	k_{on}/k_{off}
1	0.323 ± 0.008	0.065 ± 0.005	5.0 ± 0.4
2	0.028 ± 0.001	0.039 ± 0.002	0.72 ± 0.04
3	0.0141 ± 0.001	$0.914 \pm 0.026\ s^{-1}$	$0.0154 \pm 0.001\ \mu M^{-1}$
4	0.0466 ± 0.0011	0.395 ± 0.030	0.118 ± 0.009
5	0.87 ± 0.11	2.79 ± 0.02	0.31 ± 0.04

[a] Rate constants and errors were obtained from the regression analysis of stopped-flow, RFQ, and steady-state traces by the Marquardt algorithm of the program FITSIM. The units of all of the rate constants except k_{-3} are $\mu M^{-1} s^{-1}$. Units of K_3 are μM^{-1}.

In summary, the experiments described here provide strong evidence supporting the intermediacy of the paramagnetic NiFeC species in the Wood−Ljungdahl pathway. Below, we relate our kinetic results to the mechanism shown in Figure 1a. Although Scheme 1 and Figure 1a present the order of substrate binding as CO, then methyl, and then CoA, the experiments described here do not unambiguously establish this order. A rationale for this order is presented in the description of the individual steps.

Steps 1 and 2: Reduction of CODH and Reductive Activation of ACS. Two steps preceding ACS−CO formation are included in Scheme 1 to account for the first two exponential phases observed in the stopped-flow experiments in which CODH/ACS is reacted with CO. Insignificant amounts of methyl transfer from CH_3-CFeSP to ACS occur during the first ~500 ms, whereas at 390, 450, and 420 nm (not shown) the absorbance decays with rate constants of 100 and 10 s^{-1}. The rapid scanning stopped-flow results clearly show that these phases correspond to the reduction of $[Fe_4S_4]^{2+}$ clusters. The amplitudes of the first and second exponential phases correspond to approximately 1 and 0.5 $[Fe_4S_4]^{2+}$ clusters per CODH/ACS heterodimeric unit, respectively. There are three FeS clusters present in CODH (clusters B, C, and D), one in ACS (cluster A), and one in the CFeSP. Both phases must arise from clusters in CODH/ACS since they are observable in the absence of CoA and CH_3-CFeSP. Furthermore, the rate of reduction of the $[Fe_4S_4]$ cluster of the CFeSP is approximately equal to the much

slower rate of acetyl-CoA synthesis. The first step in the reaction of CODH/ACS with CO involves conversion of cluster C from C_{red1} to the C_{red2} state. This conversion, which has been followed by low-temperature EPR experiments, does not elicit a UV−visible spectral change (*25*, *46*) and occurs much faster than 100 s^{-1} (*25*). RFQ and stopped-flow kinetic studies of the CO oxidation reaction have shown that reduction of cluster B occurs with a rate constant of 100 s^{-1} (*25*, *45*, *50*). Thus, assignment of the first 100 s^{-1} phase to reduction of cluster B is fairly straightforward. Therefore, the pathway of electron flow is from CO to cluster C to cluster B; however, only cluster B reduction is observed by stopped-flow experiments in the early 100 s^{-1} phase of the reaction.

Assignment of the second cluster reduction phase, with a rate constant of ∼10 s^{-1}, is less straightforward. This rate is too slow to be involved in CO oxidation, which exhibits a k_{cat} at 25 °C of ∼100 s^{-1}. A likely possibility is that this second phase can be assigned to reduction of the $[Fe_4S]_4$ cluster in the inactive form of cluster A, in which the Ni^{2+} and $[Fe_4S_4]^{2+}$ components are not coupled. This form of cluster A is reducible by CO and other reductants to afford a high-spin ($S = {}^3/_2$) reduced cluster (*51*), which is observable by UV−visible spectroscopy and EPR. The magnitude of this rate constant is 10-fold higher than formation of the NiFeC species (0.9 s^{-1}), which means that it is not associated with the reduction of the active form of cluster A.

CO oxidation is coupled to reductive activation of cluster A in the ACS subunit. Methylation of ACS requires reductive activation of cluster A (*23*, *37*). Since cluster A is in a diamagnetic state before CO binds to form the NiFeC species, a one-electron activation of ACS is required. The formal reduction potential for the ox/red couple of the [Ni-X-Fe_4S_4] center is ∼−540 mV (*24*), although the potential required for the transmethylation reaction is probably more positive than this, since the electron-transfer and methyl-transfer reactions are coupled in an EC mechanism. Activation of cluster A involves reduction of the Ni site, not the $[Fe_4S_4]^{+2}$ cubane of cluster A (*17*), and, thus, would not be observed in the stopped-flow experiment.

Therefore, we propose that the first two steps involve the reduction of CODH, which, in turn, reduces the Ni^{2+} site in cluster A of ACS (eqs 5 and 6). The rates of oxidation and re-reduction of CODH following cluster A reductive activation occur much more rapidly than the rate of methyl transfer, so a nearly complete net reduction of cluster B is reasonable, as observed. Once cluster A undergoes activation by the intramolecular electron transfer from CODH, it can bind CO and form the paramagnetic NiFeC intermediate.

$$CODH_{ox}/ACS_{ox} + CO \rightleftarrows CODH_{red}/ACS_{ox} + CO_2 \quad (5)$$

$$CODH_{red}/ACS_{ox} + CO \rightleftarrows CODH_{red}/ACS_{red} + CO_2 \quad (6)$$

Step 3: Formation of the Paramagnetic NiFeC Species. Evidence supporting the intermediacy of the NiFeC species in the pathway is extensively discussed above. The significance of these results is that reduction of the clusters of CODH/ACS is required for acetyl-CoA synthesis and the nucleophile for the next step in the synthesis is Ni^{1+}. Interestingly, it is the Ni^{1+} form of methyl-CoA reductase that is required for reaction with methyl-coenzyme M during methanogenesis (*52*). Generally, Ni^{2+} is not a good nucleophile, but reduction to Ni^{1+} reduces the positive charge of the metal, thus enhancing its nucleophilicity. There is evidence for Ni(I) as a nucleophile in catalyzing reactions with alkyl halides (*53*, *54*). There also exists strong evidence for the reaction of Ni(I) complexes with methyl−Co(III) complexes, although, in this case, the methyl group appears to be transferred as a radical (*55*).

The studies described here also emphasize the importance of interactions between CODH and ACS to generate this low-potential intermediate during acetyl-CoA synthesis. In vivo, unless the microbes are growing on CO, the CO is generated in situ from CO_2 by the catalytic action of cluster C. The CO then migrates through a channel that connects CODH and ACS (*20*, *21*). Thus CODH and ACS must coordinate electron and carbon flow for efficient acetyl-CoA synthesis. This may be the reason that all ACS genes so far studied contain a genetically linked CODH (but not vice versa).

Step 4: Transmethylation and Subsequent Steps. The data shown herein constitute the first pre-steady-state study of the methylation of CODH/ACS and shed some light on the mechanism of methyl transfer. Our results indicate that the transmethylation step is subject to CO inhibition, a phenomenon recently described by Maynard et al. (*32*). Perhaps this inhibition affects the interaction between CODH/ACS and the CFeSP, since the CO/acetyl-CoA exchange reaction (which involves only CODH/ACS) does not exhibit inhibition by CO. Since the CO-dependent inhibition of acetyl-CoA synthesis is highly cooperative (*32*), CO inhibition of methyl transfer may not be due to simple competitive binding.

Transfer of the methyl group from the methylated CFeSP to ACS occurs at the same rate as decay of the NiFeC EPR signal. Although rates were not measured earlier, as described in the introduction, on the basis of the disappearance of the NiFeC signal when ACS−CO is reacted with a methyl donor, it was concluded that the NiFeC species is not an intermediate in the acetyl-CoA pathway (*23*, *28*). This conclusion seems reasonable since an S_N2-type transfer of the methyl group of the CH_3-CFeSP as a methyl cation to a Ni^{1+} site should yield $Co^{1+}$and the CH_3-Ni^{3+} form of ACS, which would be paramagnetic.

How can one rationalize the apparent conundrum that the Ni^{1+} form of ACS (the NiFeC species) is required for the transmethylation reaction, yet the earliest observable product of the reaction appears to be diamagnetic? The nickel site in cluster A does appear to accept the methyl group (*23*). Furthermore, there is significant evidence that this methyl transfer occurs by an S_N2 mechanism. Stereochemical studies (*31*) demonstrate a chiral methyl group from CH_3-H_4folate is incorporated into acetyl-CoA with retention of configuration. Rapid kinetic studies strongly indicate that the methyltransferase-catalyzed methylation of the CFeSP by CH_3-H_4folate is an S_N2 reaction (*56*), which implies that methylation of ACS would also result in inversion of configuration, suggesting that methylation of ACS must also occur by an S_N2 mechanism.

One could imagine an in-line Ni(I) attack on the CH_3-Co group that could result in inversion of configuration without being an S_N2 reaction. As mentioned in the previous section of the Discussion, transfer of a methyl radical would agree with the chemical precedent established by models of

the transmethylation reaction (*55*). Perhaps the transition state for the transmethylation reaction involves orbital overlap between Ni^{1+} of ACS on one side, the methyl group, and Co^{3+} on the other side. However, if the methyl group leaves formally as a methyl radical, the product must be methyl−Ni^{2+} and Co^{2+}. In contrast, our results clearly indicate that the Co^{1+}−CFeSP is the product and that there is no measurable Co^{2+} intermediate. Possibly, there is very rapid electron transfer to the Co^{2+} to form Co^{1+}. However, the rate of Co^{2+} reduction occurs at about the same rate as acetyl-CoA synthesis. Furthermore, previous studies have shown that reduction of Co^{2+}−CFeSP requires the $[Fe_4S_4]^{1+}$ cluster of the CFeSP, and crippling this cluster by mutagenesis does not affect the rate of the transmethylation reaction and the product is still Co^{1+} (*10*). It is possible perhaps that, in the transition state complex between CODH/ACS and the methylated CFeSP, a rapid one-electron transfer to Co^{2+} occurs that bypasses the $[Fe_4S_4]$ cluster of the CFeSP.

Assuming that the methyl group is transferred in an S_N2 process, how does the NiFeC signal decay to an EPR-silent species at the rate of Co^{1+} formation? Studies of the methanogenic CODH/ACS indicate that an active and associated CODH is required for the ACS-catalyzed CO/acetyl-CoA exchange reaction, which does not involve net redox chemistry (*22*). Dissociation of the α and ϵ subunits of the CODH/ACS complex from *Methanosarcina thermophila*, which constitute the CODH enzyme in this complex, leads to elimination of the exchange of carbonyl between acetyl-CoA and CO and lack of formation of the NiFeC species at the β subunit. Thus, an intramolecular electron-transfer pathway between the CODH and ACS subunits of the complex has been proposed (*22*) in which CODH reduces the methyl−Ni^{3+} product of the transmethylation reaction to methyl−Ni^{2+}. Since there is no net electron transfer during the reaction, the electron must be returned to CODH at a later stage in the catalytic cycle. Such an internal electron transfer would be expected to be fast since the NiFeC center has a low redox potential of ∼−540 mV and methyl−Ni^{3+} is expected to be a strong oxidant. Thus, there would be a strong driving force for the reaction. This proposed electron-transfer reaction coupling the CODH and ACS reactions would rationalize the conversion of a paramagnetic to a diamagnetic species during the transmethylation reaction.

The transmethylation reaction is proposed to be followed by migratory insertion of CO between the CH_3−Ni^{2+} bond to form an acetyl-ACS intermediate. ACS catalyzes a rapid CoA/acetyl-CoA exchange reaction (*57*) that follows a ping-pong mechanism (*58*), providing strong evidence for an acetyl-enzyme intermediate that binds CoA. The final steps in the mechanism include attack on the acetyl-ACS intermediate by $CoAS^-$ and, finally, release of the product, acetyl-CoA. The steps of C−S bond formation and acetyl-CoA release occur much faster than carbonylation and methylation, and they are not rate-limiting under any conditions. From previous studies of CoA exchange between acetyl-CoA and ^{32}P-labeled CoA (*57*, *59*), we estimate that C−S bond formation must have a rate constant higher than 17.5 s^{-1} at 20 °C.

Conclusions. Stopped-flow, RFQ, and steady-state kinetics and kinetic modeling experiments demonstrate the catalytic competence of the paramagnetic NiFeC species in the conversion of the methylated CFeSP, CO, and CoA to acetyl-CoA and CFeSP. This species forms and decays at rates consistent with its intermediacy in acetyl-CoA synthesis. The stopped-flow data indicate that the methyl group of the CH_3-CFeSP transferred to ACS by an S_N2 mechanism. These combined results imply that CODH/ACS follows the paramagnetic catalytic cycle described in Figure 1a in which the Ni^{1+} site of cluster A performs nucleophilic attack on the methylated CFeSP to generate a methyl−Ni^{3+} species that is rapidly reduced to form methyl−Ni^{2+}. The transmethylation reaction appears to be the step subject to CO inhibition. Subsequent steps are rapid, involving methyl migration (carbonyl insertion) to yield acetyl-ACS, which undergoes deacetylation to form acetyl-CoA.

SUPPORTING INFORMATION AVAILABLE

Two figures showing the rate of the CO/acetyl-CoA exchange reaction at different CO concentrations and the effects of titanium(III) citrate and dithiothreitol on the exchange rate. This material is available free of charge via the Internet at http://pubs.acs.org.

REFERENCES

1. Ragsdale, S. W. (1997) *BioFactors 9*, 1−9.
2. Ragsdale, S. W. (2001) in *Biological inorganic chemistry: Structure and reactivity* (Valentine, J. S., Bertini, I., and Gray, H., Eds.) University Science Books, Sausalito, CA (in press).
3. Ferry, J. G. (1999) *FEMS Microbiol. Rev. 23*, 13−38.
4. Ragsdale, S. W. (2000) in *Enzyme-catalyzed electron and radical transfer* (Holzenburg, A., and Scrutton, N., Eds.) pp 487−518, Plenum Press, New York.
5. Ragsdale, S. W. (1999) in *Chemistry and biochemistry of b12* (Banerjee, R., Ed.) pp 633−654, John Wiley and Sons, New York.
6. Lu, W.-P., Schiau, I., Cunningham, J. R., and Ragsdale, S. W. (1993) *J. Biol. Chem. 268*, 5605−5614.
7. Roberts, D. L., James-Hagstrom, J. E., Smith, D. K., Gorst, C. M., Runquist, J. A., Baur, J. R., Haase, F. C., and Ragsdale, S. W. (1989) *Proc. Natl. Acad. Sci. U.S.A. 86*, 32−36.
8. Roberts, D. L., Zhao, S., Doukov, T., and Ragsdale, S. W. (1994) *J. Bacteriol. 176*, 6127−6130.
9. Doukov, T., Seravalli, J., Stezowski, J., and Ragsdale, S. W. (2000) *Structure 8*, 817−830.
10. Menon, S., and Ragsdale, S. W. (1998) *Biochemistry 37*, 5689−5698.
11. Menon, S., and Ragsdale, S. W. (1999) *J. Biol. Chem. 274*, 11513−11518.
12. Dobbek, H., Svetlitchnyi, V., Gremer, L., Huber, R., and Meyer, O. (2001) *Science 293*, 1281−1285.
13. Drennan, C. L., Heo, J., Sintchak, M. D., Schreiter, E., and Ludden, P. W. (2001) *Proc. Natl. Acad. Sci. U.S.A. 98*, 11973−11978.
14. Ragsdale, S. W., Ljungdahl, L. G., and DerVartanian, D. V. (1982) *Biochem. Biophys. Res. Commun. 108*, 658−663.
15. Kumar, M., and Ragsdale, S. W. (1992) *J. Am. Chem. Soc. 114*, 8713−8715.
16. Ragsdale, S. W., Wood, H. G., and Antholine, W. E. (1985) *Proc. Natl. Acad. Sci. U.S.A. 82*, 6811−6814.
17. Xia, J. Q., Hu, Z. G., Popescu, C. V., Lindahl, P. A., and Munck, E. (1997) *J. Am. Chem. Soc. 119*, 8301−8312.
18. Russell, W. K., Stalhandske, C. M. V., Xia, J. Q., Scott, R. A., and Lindahl, P. A. (1998) *J. Am. Chem. Soc. 120*, 7502−7510.
19. Menon, S., and Ragsdale, S. W. (1996) *Biochemistry 35*, 12119−12125.
20. Seravalli, J., and Ragsdale, S. W. (2000) *Biochemistry 39*, 1274−1277.
21. Maynard, E. L., and Lindahl, P. A. (1999) *J. Am. Chem. Soc. 121*, 9221−9222.

22. Murakami, E., and Ragsdale, S. W. (2000) *J. Biol. Chem. 275*, 4699−4707.
23. Barondeau, D. P., and Lindahl, P. A. (1997) *J. Am. Chem. Soc. 119*, 3959−3970.
24. Gorst, C. M., and Ragsdale, S. W. (1991) *J. Biol. Chem. 266*, 20687−20693.
25. Kumar, M., Lu, W.-P., Liu, L., and Ragsdale, S. W. (1993) *J. Am. Chem. Soc. 115*, 11646−11647.
26. Lindahl, P. A., Münck, E., and Ragsdale, S. W. (1990) *J. Biol. Chem. 265*, 3873−3879.
27. Wilson, B. E., and Lindahl, P. A. (1999) *J. Biol. Inorg. Chem. 4*, 742−748.
28. Grahame, D. A., Khangulov, S., and Demoll, E. (1996) *Biochemistry 35*, 593−600.
29. Grahame, D. A., and Demoll, E. (1995) *Biochemistry 34*, 4617−4624.
30. Lu, W. P., Harder, S. R., and Ragsdale, S. W. (1990) *J. Biol. Chem. 265*, 3124−3133.
31. Lebertz, H., Simon, H., Courtney, L. F., Benkovic, S. J., Zydowsky, L. D., Lee, K., and Floss, H. G. (1987) *J. Am. Chem. Soc. 109*, 3173−3174.
32. Maynard, E. L., Sewell, C., and Lindahl, P. A. (2001) *J. Am. Chem. Soc. 123*, 4697−4703.
33. Andreesen, J. R., Schaupp, A., Neurater, C., Brown, A., and Ljungdahl, L. G. (1973) *J. Bacteriol. 114*, 743−751.
34. Ragsdale, S. W., Clark, J. E., Ljungdahl, L. G., Lundie, L. L., and Drake, H. L. (1983) *J. Biol. Chem. 258*, 2364−2369.
35. Ragsdale, S. W., Lindahl, P. A., and Münck, E. (1987) *J. Biol. Chem. 262*, 14289−14297.
36. Elliott, J. I., and Brewer, J. M. (1978) *Arch. Biochem. Biophys. 190*, 351−357.
37. Lu, W.-P., Harder, S. R., and Ragsdale, S. W. (1990) *J. Biol. Chem. 265*, 3124−3133.
38. Ragsdale, S. W., and Wood, H. G. (1985) *J. Biol. Chem. 260*, 3970−3977.
39. Raybuck, S. A., Bastian, N. R., Orne-Johnson, W. H., and Walsh, C. T. (1988) *Biochemistry 27*, 7698−7702.
40. Ballou, D. P. (1978) *Methods Enzymol. 54*, 85−93.
41. Seravalli, J., Brown, K. L., and Ragsdale, S. W. (2001) *J. Am. Chem. Soc. 123*, 1786−1787.
42. Roberts, J. R., Lu, W.-P., and Ragsdale, S. W. (1992) *J. Bacteriol. 174*, 4667−4676.
43. Hogenkamp, H. P., Bratt, G. T., and Sun, S. Z. (1985) *Biochemistry 24*, 6428−6432.
44. Kumar, M., Qiu, D., Spiro, T. G., and Ragsdale, S. W. (1995) *Science 270*, 628−630.
45. Seravalli, J., Kumar, M., Lu, W.-P., and Ragsdale, S. W. (1997) *Biochemistry 36*, 11241−11251.
46. Anderson, M. E., and Lindahl, P. A. (1996) *Biochemistry 35*, 8371−8380.
47. Hu, Z. G., Spangler, N. J., Anderson, M. E., Xia, J. Q., Ludden, P. W., Lindahl, P. A., and Münck, E. (1996) *J. Am. Chem. Soc. 118*, 830−845.
48. Shin, W., Anderson, M. E., and Lindahl, P. A. (1993) *J. Am. Chem. Soc. 115*, 5522−5526.
49. Barshop, B. A., Wrenn, R. F., and Frieden, C. (1983) *Anal. Biochem. 133*, 134−145.
50. Seravalli, J., Kumar, M., Lu, W. P., and Ragsdale, S. W. (1995) *Biochemistry 34*, 7879−7888.
51. Xia, J. Q., Dong, J., Wang, S. K., Scott, R. A., and Lindahl, P. A. (1995) *J. Am. Chem. Soc. 117*, 7065−7070.
52. Goubeaud, M., Schreiner, G., and Thauer, R. K. (1997) *Eur. J. Biochem. 243*, 110−114.
53. Lahiri, G. K., and Stolzenberg, A. M. (1993) *Inorg. Chem. 32*, 4409−4413.
54. Hevelston, M., and Castro, C. (1992) *J. Am. Chem. Soc. 114*, 8490−8496.
55. Ram, M. S., Riordan, C. G., Yap, G. P. A., LiableSands, L., Rheingold, A. L., Marchaj, A., and Norton, J. R. (1997) *J. Am. Chem. Soc. 119*, 1648−1655.
56. Zhao, S., Roberts, D. L., and Ragsdale, S. W. (1995) *Biochemistry 34*, 15075−15083.
57. Ramer, S. E., Raybuck, S. A., Orme-Johnson, W. H., and Walsh, C. T. (1989) *Biochemistry 28*, 4675−4680.
58. Bhaskar, B., DeMoll, E., and Grahame, D. A. (1998) *Biochemistry 37*, 14491−14499.
59. Lu, W. P., and Ragsdale, S. W. (1991) *J. Biol. Chem. 266*, 3554−3564.

BI011687I